Embedded-atom model of glass-forming Si-metal alloys

Pietro Ballone
Institut für Festkörperforschung, Forschungszentrum Jülich, D-52425 Jülich, Germany

Silvia Rubini
Dipartimento di Fisica "Alessandro Volta," Università di Pavia, via Bassi 6, I-27100 Pavia, Italy
(Received 23 November 1994)

We develop and test an embedded-atom model for late transition-metal (Ni, Pd, Pt and Au)–silicon alloys with Si concentration up to 20 at.%. We exploit the model to simulate by molecular dynamics the quench from high temperature of $Ni_{80}Si_{20}$, $Pd_{80}Si_{20}$, $Pt_{80}Si_{20}$, and $Au_{80}Si_{20}$ that results in the formation of an amorphous system in the case of the Pd-Si, Pt-Si, and Au-Si alloys. We analyze in detail the glass transition and the variation across it of the viscosity and diffusion coefficient. Moreover, we study the static structure and the elastic and vibrational properties of the low-temperature amorphous alloys. The results show that, despite some quantitative disagreement, the embedded-atom potential reproduces all the major features and trends observed in the experiments, and provides a reliable model for the simulation of these systems.

INTRODUCTION

Metallic glasses are fascinating materials with promising perspectives in catalysis, high-strength materials, and magnetic applications.[1] Together with more common glasses (silicates, chalcogenides, and polymers) they challenge our ability to describe the structure and atomic dynamics of systems out of equilibrium.[2] Fundamental and not fully answered questions concern the exact nature of the glass transition, the behavior of dynamical and transport properties close to the glass temperature T_g, and the relaxation processes occurring at lower temperature.[3]

Three major classes of metallic glasses have been experimentally investigated.[4] The first class, exemplified by $Cu_{60}Zr_{40}$ and $Ni_{24}Zr_{76}$, contains alloys of early transition metals (TM's) with late TM's. The second one, composed of alloys of simple metals and early TM's, has received considerable attention because of the potential applications of Al-TM alloys, like $Al_{87}Y_8Ni_5$. The last and most important class includes the alloys of late TM's or noble metals with a metalloid (mainly B, Si, P), and is exemplified by $Au_{80}Si_{20}$, $Pd_{80}Si_{20}$, $Fe_{80}B_{20}$, and $Ni_{80}P_{20}$.

An increasing role in the theoretical investigation of these systems has been played by computer simulation, and in particular by molecular dynamics (MD), because of the ease in obtaining glasses by this method, its microscopic resolution in the determination of structural and dynamical properties, and the possibility of performing "computer experiments" unfeasible in the real world. Needless to say, these positive features are partially compensated by the intrinsic limitations of MD to small systems and short times, which may prevent the direct simulation of several phenomena relevant for glasses.

A crucial ingredient of any investigation of glasses by computer simulation is the underlying model for the system potential energy. Pioneering investigations exploited simple interatomic potentials (hard spheres,[5] and Lennard-Jones[6] and inverse power potentials[7]), for which the equilibrium properties were well known, and that, because of their idealized form, were well suited to highlight the unifying features of glasses. Quantitative studies, however, require more refined potentials, especially to investigate properties that are not universal, but dependent on the specific system under study.

Most of the MD simulations aiming at the realistic description of specific systems have been devoted to simple metal-TM and TM-TM alloys, mainly because of the availability of potential energy models already tested for equilibrium conditions. In order of increasing complexity (but not always accuracy), we mention pair potential models, perturbation theory based on the homogeneous electron gas, embedded-atom (EA) models, and tight-binding (TB) schemes. Pair potentials are computationally very convenient, and still able to reproduce several structural and dynamical properties of metallic glasses.[8] Reliable models, however, are density (and thus state) dependent, and the fitting procedure to determine the pair interaction can be cumbersome. Moreover, these models are usually unsuited to study inhomogeneous systems like surfaces and interfaces. The metallic character of alloys of simple metals is better reflected by perturbation theory based on the electron gas,[9] which has been extensively used to model, for instance, Mg-Zn,[10] Ca-Mg,[11] and Ca-Al alloys.[12] This scheme, however, cannot be extended to TM's, and shares with pair potentials the limitation to nearly homogeneous systems.

Tight-binding models for metallic glasses, developed mainly by Hafner and collaborators,[13] are potentially one step beyond the other schemes, since they include explicitly information on the electronic structure of the system, and have been applied to model TM-TM (Refs. 13, 14) and TM-metalloid amorphous alloys.[15] However, at least in the implementations presented until now, TB schemes appear also rather complex, and some of the assump-

tions are less transparent and easily verified than those at the basis of other methods. Moreover, for what concerns the static structure and the vibrational properties, the agreement between theory and experiment achieved by this method does not appear to be clearly superior to that of the others.

Embedded-atom methods,[16,17] finally, seem to represent the best compromise of computational simplicity, flexibility, and accuracy for metallic systems, and, therefore, have been used to model TM-TM glasses,[18] and, to a minor extent, simple metal-TM alloys.[19]

In the present study we develop an EA scheme to model TM-Si glass-forming alloys. The basis for our model is provided by the experimental observation that these alloys are apparently metals and that the Si atoms do contribute to the metallic bonding, provided the Si concentration does not exceed ~ 30 at.%. This point of view is supported by photoemission spectroscopy,[20] electrical conductivity measurements, reflectance spectra,[21] and calorimetry.[22] All these observations justify the extension to these systems of a scheme explicitly tailored for metallic systems. In our model we emphasize the ability of the potential to provide a global and robust description of these alloys with the minimum of fitting parameters, in view of an extensive exploitation for systems (like defects, surfaces, and ternary alloys) rather far from those used to fit the potential. This transferability property is achieved at the cost of some quantitative disagreement between computed and measured radial distribution functions, which, however, is still comparable or even better than that achieved by previous studies. A fine tuning of the potential could surely improve significantly this comparison for any specific application. At variance with previous EA potentials for Si (Refs. 23, 24) that aimed at the description of the full variety of metallic and semiconducting phases of this element, we carefully restrict the application range of our model to metallic systems. This restriction allows us to retain the simplicity and computational appeal of the original EA scheme.

As an extensive test of the model we simulate by MD the quench from high temperature of $Ni_{80}Si_{20}$, $Pd_{80}Si_{20}$, $Pt_{80}Si_{20}$, and $Au_{80}Si_{20}$, which results in the formation of an amorphous system in the case of the Pd-, Pt-, and Au-Si alloys. The analysis of thermodynamic and transport properties, the static structure, and the dynamics close to T_g and at low temperature confirms that the EA potential describes reliably all the major features of these systems. Of course, the real value of the model is not in its ability to reproduce these rather well-known properties, but in its possible applications to investigate at the atomistic level (although not necessarily by MD) a variety of processes, like diffusion, low-energy excitations, and relaxation, not fully understood in real systems.

EA MODEL

To enhance the transferability of our Si potential to a wide class of metallic alloys, we devised and tested the following procedure. First, we produced the EA potentials for a series of simple and transition metals (Al, Ni, Pd, Pt, Au), gauging the cross interactions on several intermetallic alloys among these elements. Second, we generated the potential for Si following the scheme described below. Third, we determined the alloying properties of metallic Si by fitting the lattice constants of the fcc Al:Si random alloy.[25] In this stage of the fit the alloy properties of Si with the other metals were not used. Finally, we verified that the Si potential obtained in this way can be combined (without further fitting) with any of the potentials in the (Ni, Pd, Pt, Au) set to provide a reliable description of their alloys with up to $\sim 20\%$ of Si. This test, which is the main subject of the present section, demonstrates a fair degree of transferability for the Si potential over a set of consistently generated metal potentials. As a consequence, we expect that our potential can also be used (at least at a semiquantitative level) to study Si alloys with other metals M, even if a direct fit of M:Si properties cannot be performed (for instance for lack of experimental data). To this aim, it could be sufficient to harmonize the M potential with those of the metals discussed below.

The special role of Al in fitting the alloying properties of Si was motivated by the similarity in the atomic volume of Al and metallic Si, and by the more general equivalence we expected for the metallic phases of these *sp* elements occupying two successive positions in the periodic table.

As extensively described in the original papers,[16] the EA potential for a set of N atoms is written as

$$E = \sum_{i<j}^{N} \varphi_{i,j}(r_{ij}) + \sum_{i}^{N} F_i[\rho(\vec{r}_i)], \tag{1}$$

where $\varphi_{i,j}$ is a short-range, repulsive pair potential, and F_i is the energy gain in embedding the atom i into the electron density $\rho(\vec{r}_i)$.

In the following, we assume

$$\varphi_{i,j}(r) = Z_i(r)Z_j(r)/r, \tag{2}$$

with

$$Z_i(r) = Z_0^i(1+\beta_i r^{\nu_i})\exp(-\alpha_i r), \tag{3}$$

where Z_0^i, α_i, β_i, and ν_i are free parameters. Moreover, the embedding density $\rho(\vec{r}_i)$ is the superposition of atomiclike contributions $\rho^{(\mathrm{at})}$ from all the other atoms in the system:

$$\rho(\vec{r}_i) = \sum_j \rho_j^{(\mathrm{at})}(|\vec{r}_i - \vec{r}_j|). \tag{4}$$

In turn, $\rho^{(\mathrm{at})}(r)$ is written as the sum of contributions coming from two orbitals $\Psi_\alpha(r)$ and $\Psi_\beta(r)$ of different symmetry:

$$\rho^{(\mathrm{at})}(r) = n_\alpha |\Psi_\alpha(r)|^2 + (N_v - n_\alpha)|\Psi_\beta(r)|^2, \tag{5}$$

where N_v is the valence charge of the element, and n_α is a free parameter. For transition metals α and β correspond

to s and d symmetry, respectively, while s and p orbitals are considered for Al and Si.

Both the $Z(r)$ and the Ψ's have been cut at a cut off distance R_c, and a shift has been applied to obtain a potential that is continuous and has a continuous first derivative everywhere.

For the metals listed above our fit to the properties of the single elements is standard, and we simply report in Table I the elastic constants and vacancy formation energy for reasons of reproducibility and test. The lattice parameter, cohesive energy, and bulk modulus used in our fit are those reported in Ref. 26.

In the Appendix we describe in some more detail the generation of the EA potential for Si, since the low-pressure, low-temperature diamond phase is nonmetallic, and clearly outside the validity range of the simplest EA scheme.

The role of n_α in determining the properties of alloys has been discussed extensively. Here we simply remark that our recipe to fit n_α is slightly different from the one described in the original paper on the EA modeling of alloys,[26] which used the properties of dilute impurities to determine the cross interactions, and focused on the enthalpy of mixing instead of structural properties. We choose to determine n_α from the properties of intermetallic compounds because we expected this to be more reliable for alloys of finite concentration. In fact, by comparing for a few cases the potentials obtained by fitting the properties of impurities and intermetallic compounds we concluded that the two choices produce equivalent potentials. We decided to fit structural data because these are available for a large number of intermetallic at low T. Enthalpy, instead, is usually tabulated only for high T, and this makes less straightforward or less reliable its usage in the fit. Moreover, in our experience the lattice constant and excess enthalpy of alloys are, to a large extent, equivalent properties in the EA potential: Larger lattice constants usually imply lower mixing enthalpy, and fitting one or the other property provides again equivalent potentials.

TABLE I. Elastic constants C_{ij} and vacancy formation energy E_v of the EA potential for the pure metals and for sc Si. The numbers in parentheses are the experimental values for the metals reported in Ref. 26, and the results of *ab initio* computations for Si (Ref. 27; see text).

Element	C_{11} (Mbar)	C_{12} (Mbar)	C_{44} (Mbar)	E_v (eV)
Al	1.01	0.71	0.46	0.87
	(1.12)	(0.66)	(0.28)	(0.7)
Ni	2.33	1.54	1.28	1.64
	(2.46)	(1.47)	(1.25)	(1.6)
Pd	2.24	1.81	0.73	1.47
	(2.34)	(1.76)	(0.71)	(1.4)
Pt	3.11	2.69	0.74	1.51
	(3.47)	(2.51)	(0.77)	(1.5)
Au	1.85	1.58	0.43	0.88
	(1.86)	(1.57)	(0.42)	(0.9)
Si	2.10	0.51	0.20	-
	(2.23)	(0.44)	(0.20)	-

The optimal potential parameters are collected in Table II.

The comparison of the computed and experimental lattice parameters for a series of intermetallic compounds is reported in the first half of Table III. This comparison is focused on the alloys containing Al because of the similarity with metallic Si mentioned above. As apparent from a survey of crystallographic data, the alloys of Al with transition metals tend to have complex structures, deformed by long-range oscillatory interactions that can be traced to Fermi surface effects.[30] The size of the distortion depends on the transition metal (for instance, it is larger for Pd than for Ni) and decreases with decreasing Al content. The most distorted structures (like those of Pd_2Al and $AuAl_2$) are not reproduced quantitatively by the EA potential (at least in the form we use), which does not contain the long-range Friedel oscillations of the interatomic potential. The relaxed structures obtained within the EA potential tend to be a symmetrized version of the experimental ones, of which they retain some basic properties like the equilibrium volume and the number of neighbors. As discussed below, the same trends are observed in the intermetallic compounds of Si. The comparison of computed excess internal energies of mixing at $T = 0$ with the excess enthalpy at $T \sim 300$ K (also reported in Table III) suggests that the model is able to reproduce the experimental trends, again with the notable exception of $AuAl_2$.

Among the metals considered above, Ni, Pd, and Pt form ordered intermetallic compounds $M_{1-x}Si_x$ with Si, few of which have $x \leq 0.30$, and are, therefore, within the reach of the EA potential. We used these systems for a first test of the reliability of our potentials. The results are reported in the second part of Table III. Two regularities are apparent. First, and not surprisingly, the accuracy of the potential increases with decreasing x, as shown by the comparison of the Ni_2Si and Ni_3Si results. Second, the chemical trends observed for $M_{1-x}Al_x$ remain in $M_{1-x}Si_x$: The elements like Pd (and, to a minor extent, Pt) that form complex structures with Al give rise to complex unit cells also with Si, with distortions that are not quantitatively reproduced by EA.

GLASS TRANSITION

With the potentials described above we simulated by MD the quench from the melt for samples of $Ni_{80}Si_{20}$, $Pd_{80}Si_{20}$, $Pt_{80}Si_{20}$, and $Au_{80}Si_{20}$. In real experiments

TABLE II. Embedded-atom potential parameters used in the simulation.

	Z_0 (e)	α (Å^{-1})	β (Å^{-1})	ν	N_s	R_c (Å)
Al	3	1.315	3.781	0.326	1.90	5.5
Ni	10	1.863	0.896	1.000	1.78	4.8
Pd	10	1.295	0.593	−2.913	1.70	5.5
Pt	10	1.639	0.802	0.603	1.67	5.5
Au	11	1.548	0.501	0.131	1.18	5.5
Si	3.2	0.551	298.353	−8.906	0.8	4.8

TABLE III. Lattice parameters a, b, c and excess internal energy of mixing $\Delta U^{\rm mix}$ at $T = 0$ for selected M-Al and M-Si alloys (M=Ni, Pd, Pt, and Au). The $\Delta U^{\rm mix}$ for the Si alloys has been computed with respect to the experimental cohesive energy of diamond Si. The experimental values for the lattice parameters (in parentheses) are from Ref. 28, the excess enthalpies of mixing ΔH are from Ref. 29.

Alloy	Structure	a (Å)	b (Å)	c (Å)	$\Delta\ U^{\rm mix}$ (eV/atom)
NiAl	CsCl	2.92	-	-	−0.49
		(2.89)	-	-	($\Delta\ H = -0.61$, $T = 298$ K)
Ni_3Al	Cu_3Au	3.57	-	-	−0.39
		(3.57)	-	-	($\Delta\ H = -0.39$, $T = 298$ K)
PdAl	CsCl	3.04	-	-	−0.91
		(3.04)	-	-	($\Delta\ H = -0.96$, $T = 373$ K)
Pd_2Al	Pd_2Al	5.34	3.92	8.01	−0.77
		(5.41)	(4.06)	(7.77)	($\Delta\ H = -0.88$, $T = 373$ K)
$PtAl_2$	CaF_2	5.94	-	-	−0.36
		(5.92)	-		
Pt_3Al	Ni_3Al	3.85	-	-	−0.75
		(3.88)	-	-	($\Delta\ H = -0.72$, $T = 298$ K)
$AuAl_2$	CaF_2	6.27	-	-	−0.01
		(6.01)	-	-	($\Delta\ H = -0.44$, $T = 400$ K)
Au_2Al	$MoSi_2$	3.38	-	8.84	−0.34
		(3.35)	-	(8.89)	($\Delta\ H = -0.36$, $T = 400$ K)
Ni_3Si	Cu_3Au	3.45	-	-	−0.64
		(3.51)	-	-	-
Ni_2Si	$PbCl_2$	7.21	4.78	3.47	−0.80
		(7.06)	(4.99)	(3.72)	-
Pd_3Si	Fe_3C	5.31	7.51	5.31	−0.84
		(5.74)	(7.56)	(5.26)	-
Pt_3Si	Pt_3Ge	7.60	-	7.60	−0.90
		(7.70)	-	(7.77)	-

these systems can be divided into two categories. On the one hand, the Pd- and Au-Si alloys, which give rise to few or no intermetallic compounds, are easily produced in the glassy state, with estimated critical cooling rates of the order of 10^4 K/sec. On the other hand, the Si alloys of Ni and Pt, which do form several ordered intermetallic compounds, are not frozen in the glassy phase by comparable cooling rates: $Pt_{80}Si_{20}$ can be prepared in the glassy state only by laser quenching, but not by the slower splat cooling, while $Ni_{80}Si_{20}$ crystallizes even under the fastest experimental quenching conditions and its amorphous form is obtained only by nonthermal processes like sputtering. The minimum quenching rate we can achieve in our simulation is still one or two orders of magnitude faster than the fastest experimental one. It is interesting to observe that, despite this limitation, our computation is able to reproduce the different behavior of the alloys listed above, and to provide a description at least qualitatively correct of the glass transition in the Pd-, Pt-, and Au-Si alloys.

The MD simulation was performed for systems of 864 atoms in a cubic box with periodic boundary conditions. The equations of motion have been integrated by a velocity Verlet algorithm[31] with a time step of 1.571×10^{-15} sec. Each simulation was started by equilibrating the system at very high temperature ($T > 2000$ K), at which the alloys were liquid. Then, we decreased T by discontinuous jumps of less than 100 K each. After each variation of T we reequilibrated the system during 10^4 MD steps (16 psec) and the volume was carefully calibrated to follow the zero-pressure equation of state. Statistics was accumulated during runs of 10^5 steps (0.16 nsec). Each quench, therefore, lasted more than 2×10^6 steps, or 3.2 nsec, corresponding to a cooling rate of 0.8 10^{12} K/sec, which has to be compared with the 10^{10} K/sec achieved by laser quenching, and the much slower 10^7 K/sec obtained by the fastest mechanical quenching methods.[32] Our results, therefore, approach those of laser quenching, while providing only a rough approximation for splat cooling. The long equilibration and statistics runs and the small jumps in T ensure that the results do not depend much on the details of the cooling schedule, although they do depend on the global cooling rate, as shown by the glassy state obtained below T_g. We did not apply constant-T and constant-P MD algorithms because these modify the dynamics of the system, which is, instead, one of the aims of the present computation. Constant-pressure MD (Parrinello-Rahman[33]) has been used to test the structural stability of the glassy samples at the end of the quench.

The first quantity we discuss is the internal energy $U(T)$ during the cooling, reported in Fig. 1 for $Pd_{80}Si_{20}$. The points are the average of the potential energy over the 10^5 step statistics runs. With the cooling rate of our simulation, the Pd, Pt, and Au alloys display the discontinuity in the slope of $U(T)$ that signals the glass transition, without any discontinuity in $U(T)$ itself that would be associated with crystallization in at least a part of the system. The Ni-Si alloy behaves in a different way: At $T \sim 1500$ K it crystallizes in a (defective) fcc structure

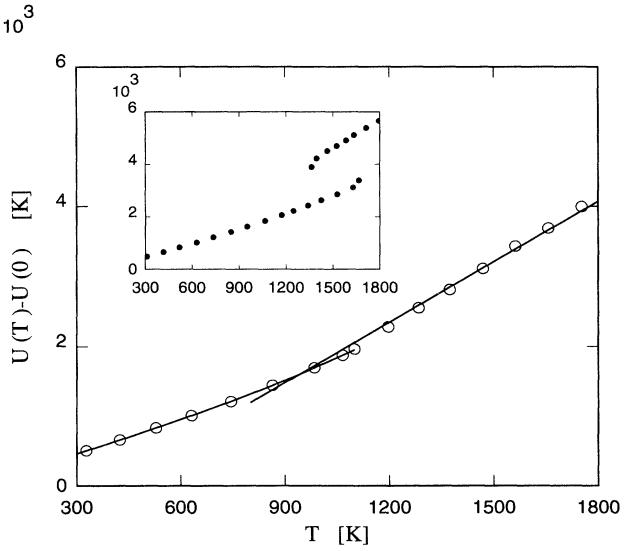

FIG. 1. Internal energy per atom U as a function of T during cooling at a rate of 0.8×10^{-12} K/sec. Main plot: $Pd_{80}Si_{20}$; inset: $Ni_{80}Si_{20}$. The points are averages over 0.16 nsec microcanonical runs. The zero of U is given by the energy of the fcc random alloy.

(see the inset of Fig. 1). Also this alloy can be obtained in a glassy structure by an abrupt quench from the liquid.

The quantitative determination of the glass transition has been performed by fitting $U(T)$ by the Pade' form

$$U(T) = \frac{a + bT + cT^2}{1 + dT}, \tag{6}$$

with two different sets of coefficients for the low-and high-T portion of $U(T)$. The subdivision of the temperature range in a low- and high-T portion is decided *a priori* by visual inspection of the simulation results, and excludes the data close to the point where $U(T)$ changes slope. The transition temperature T_g has been determined from the intersection of the low- and high-T interpolation of $U(T)$. A similar fit has been performed for the zero pressure volume $V(T)$. This provides a nearly identical estimate of T_g. The estimated T_g, together with the discontinuities in the constant-pressure specific heat C_p and isobaric thermal expansion coefficient $\alpha_P = (\partial V/\partial T)_P/V$, are reported in Table IV. The comparison with experimental systems is hampered by the scarcity of data on T_g for metallic glasses. By considering the experimental T_g for $Pd_{82}Si_{18}$ and the crystallization temperature T_c for the other alloys (and taking into account that $T_g \geq T_c$),[4] we estimate that our EA model overestimates T_g by ~ 200 K. Part of the discrepancy is probably due to the fast quench imposed by MD, since experiments and simple qualitative arguments show that T_g increases with increasing cooling rate. Most of the discrepancy, however, is likely to be due to the inaccuracies in the potential, which are reflected also on the static structure and dynamical properties, as discussed below.

The most common definition of T_g is in terms of dynamical properties like the viscosity $\eta(T)$ and the diffusion coefficient $D(T)$. We computed η by the Green-Kubo relation

$$\eta(T) = \frac{\rho}{Nk_BT}\int_0^\infty \chi(t)dt, \tag{7}$$

where ρ is the number density, N the total number of atoms in the system, and χ is the time autocorrelation function of the shear stress σ_{xy}:

$$\chi(t) = \langle \sigma_{xy}(t+s)\sigma_{xy}(s)\rangle.$$

In turn, the stress tensor $\sigma_{\alpha,\beta}$ is defined by

$$\sigma_{\alpha\beta} = \sum_i \sigma^{(i)}_{\alpha,\beta} = \sum_i \frac{1}{2}\left(\sum_{j\neq i} \vec{f}_{ij}(\vec{r}_i - \vec{r}_j) + 2m_i\vec{v}_i^{\alpha}\vec{v}_i^{\beta}\right), \tag{8}$$

where α, β are Cartesian coordinates, $\vec{f}_{ij}$ is the force on atom i due to atom j, $\vec{v}_i$ is the velocity, and m_i the mass of atom i.

The computation of η is notoriously difficult, and our data are affected by large error bars, which increase with decreasing T (from $\sim 20\%$ at $T \geq 2000$ K to $\sim 30\%$ at $T \sim 1.2T_g$). Our results for $Pt_{80}Si_{20}$ are reported in Fig. 2. Despite the error bars, it is possible to recognize a clear Arrhenius behavior of the computed $\eta(T)$ in the liquid phase, down to $1.2T_g$. For lower T our results become unreliable, since the length of the simulation (0.16 nsec, extended to 0.50 nsec for few systems close to T_g) is not sufficient to cover the long time tail in $\chi(t)$, which contributes significantly to η. Therefore, our discussion of the crossover from the Arrhenius to the Vogel-Fulcher form, expected close to T_g, is only tentative. Our results [together with the data for $D(T)$ discussed below] suggest that η changes rather smoothly across T_g, at least on the nsec time scale, before a significant relaxation reduces drastically both η and D. A fit with the Vogel-Fulcher relation

$$\ln\eta = A + \frac{B}{T - T'} \tag{9}$$

TABLE IV. Glass transition temperature T_g, zero-pressure specific heat C_p (potential energy contribution only), and thermal expansion coefficient α_P evaluated in the amorphous (T_g^-) and undercooled liquid (T_g^+) phases at $T = T_g$.

	T_g (K)	$C_p(T_g^-)/k_B$	$C_p(T_g^+)/k_B$	$\alpha_P(T_g^-)$ (K^{-1})	$\alpha_P(T_g^+)$ (K^{-1})
$Pd_{80}Si_{20}$	943	2.13	2.88	1.334×10^{-5}	2.817×10^{-5}
$Au_{80}Si_{20}$	403	1.73	2.51	1.701×10^{-5}	3.430×10^{-5}
$Pt_{80}Si_{20}$	930	1.66	2.76	1.117×10^{-5}	2.040×10^{-5}

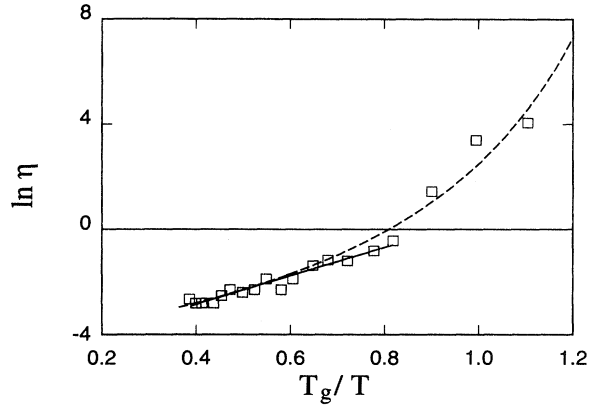

FIG. 2. Viscosity coefficient as a function of inverse T for $Pt_{80}Si_{20}$. Squares: simulation results. Solid line: Arrhenius fit for the liquid phase. Dashed line: fit by a Vogel-Fulcher-type relation (see text).

is still possible, but provides a value for T' that is only one half of the T_g we estimate from the slope of $U(T)$. The origin of this behavior is, again, in the short simulation length. A relaxation over macroscopic times would increase η by orders of magnitude, and reconcile the estimate of the glass temperature from η (and D; see below) with that from $U(T)$.

A complementary description of the system transformation approaching T_g is provided by the diffusion coefficient $D(T)$, which has been computed by a linear fit to the long time behavior of the mean square atomic displacement:

$$D = \lim_{t\to\infty} \left\langle \frac{1}{N}\sum_{i=1}^{N} | r_i(t) - r_i(0) |^2 \right\rangle \Big/ 6t. \qquad (10)$$

The data for Au and Si in $Au_{80}Si_{20}$ are reported in Fig. 3 on a scale that highlights the Arrhenius form $D(T) = D_0 \exp(-\Delta E/K_b T)$ for $T > T_g$. From the plots of $D(T)$ it is possible to estimate the preexponential factor D_0 and the apparent barrier ΔE in the liquid phase, which are listed in Table V. Comparison with the experimental values reported in Ref. 34 shows that the orders of magnitude and the trends are correct. Also in agreement with the experimental determinations is the fact that Si diffuses more slowly than the metals,[35] despite the large advantage in mass. It is tempting to interpret this fact by assuming that in the liquid phase Si diffuses together with a cage of metal neighbors, which are the precursors of the structural units described in the following section. Analysis of atomic trajectories, however, shows that the behavior of the Si and the metal atoms is similar, with only quantitative differences. This has been shown by identifying the nearest neighbor (NN) shell of few Si and metal atoms, and analyzing how often one atom is replaced in this first coordination shell. We observe that at $T \sim 1.2T_g$ every atom interchanges at least one of its NN's within 20 psec, and the process is only slightly slower for Si than for the metals.

Comparison of our results for $D(T)$ with a power law inspired by mode coupling theory,[36]

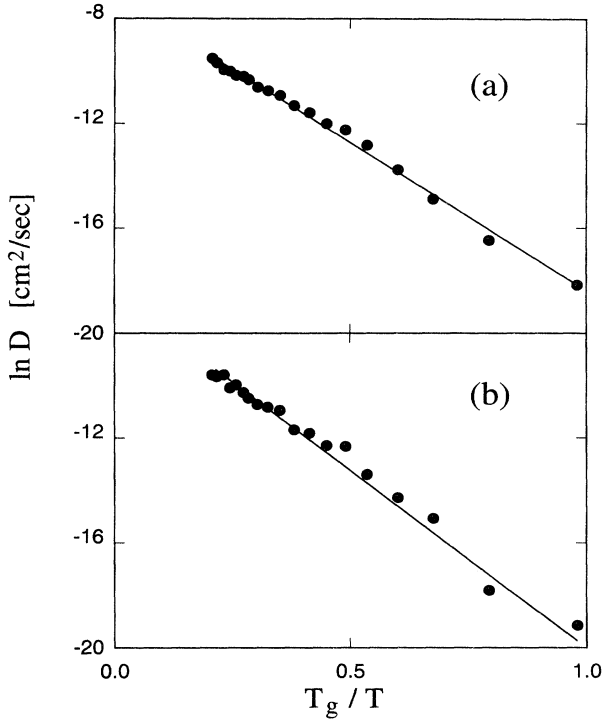

FIG. 3. Diffusion coefficient of (a) Au atoms and (b) Si atoms in $Au_{80}Si_{20}$ as a function of inverse temperature. The solid line is an Arrhenius fit to the simulation results.

$$D(T) = A(T - T')^{\alpha}, \qquad T > T', \qquad (11)$$

highlights two major points. As mentioned above, and as remarked by several previous investigations, $D(T)$ does not vanish at T_g, although at lower temperatures it has a value that can hardly be measured by MD. Disregarding this qualitative discrepancy, the fit of $D(T)$ with Eq. (11) is almost as good as that obtained with the Arrhenius form, and a distinction of the two is difficult to achieve with the accuracy allowed by simulation. Again, the optimal T' is somewhat lower than the T_g computed from $U(T)$ (see also Ref. 37 for a similar observation). As a last remark, we notice that both the diffusion coefficients of Si and the metal can be fitted by Eq. (11) with the same T', and with a slightly different α.

Another theory of diffusion we considered in the interpretation of our results is the so-called "free volume" theory,[38] which predicts an exponential dependence of D on the volume:

$$D(T) = D_0 \exp[-bv_0/(v - v_0)], \qquad (12)$$

where v is the mean atomic volume, and v_0 is the close packing volume of the atoms (i.e., the volume at which no residual diffusion remains). Assuming D_0, b, and v_0 as free parameters, this relation provides probably the best fit of our results over the entire simulation range. The same value of v_0 (but not of D_0 and b) provides an excellent fit of the diffusion coefficient for the undercooled liquid as a function of pressure at constant T, as we verified by a series of simulations for $Au_{80}Si_{20}$ at 895

TABLE V. Preexponential parameter D_0 and energy barrier ΔE of an Arrhenius fit ($D(T) = D_0 \exp[-\Delta E/k_B T]$) for the liquid phase diffusion of metal (M) and Si atoms.

	$D_0(M)$ (cm^2/sec)	$\Delta E(M)$ (K)	D_0(Si) (cm^2/sec)	ΔE (Si) (K)
$Au_{80}Si_{20}$	5.01×10^{-4}	3888	6.53×10^{-4}	4323
$Pd_{80}Si_{20}$	9.18×10^{-4}	6766	9.73×10^{-4}	7322
$Pt_{80}Si_{20}$	7.01×10^{-4}	6909	8.95×10^{-4}	7921
$Ni_{80}Si_{20}$	1.95×10^{-3}	7511	2.35×10^{-4}	8510

K under pressures ranging up to 90 kbar.

Below T_g our estimate for $D(T)$ is affected by large statistical errors. The main conclusion we can draw from our simulation is that a residual diffusion remains below T_g, without any tendency to vanish over a nsec time scale (the longest constant-temperature run performed below T_g reached 10^6 steps, or 1.6 nsec). The atomic processes contributing to the residual diffusion in the amorphous alloys appear to be different from those characterizing the diffusion in hot crystalline solids. This difference is highlighted again by comparison with the behavior of the $Ni_{80}Si_{20}$ defective crystal obtained by our quench. Figure 4 reports the time evolution of the square displacement per atom Δr^2 from an arbitrary, well-equilibrated configuration in $Ni_{80}Si_{20}$ at $T = 1341$ K (a) and in $Au_{80}Si_{20}$ at $T = 398$ K. The plot for $Ni_{80}Si_{20}$ displays one of the few jumps we observed for this system at a T below the first-order transition. The jump involves several atoms (about ten, including both Ni and Si) and is abrupt. The behavior of $Au_{80}Si_{20}$ is apparently different:

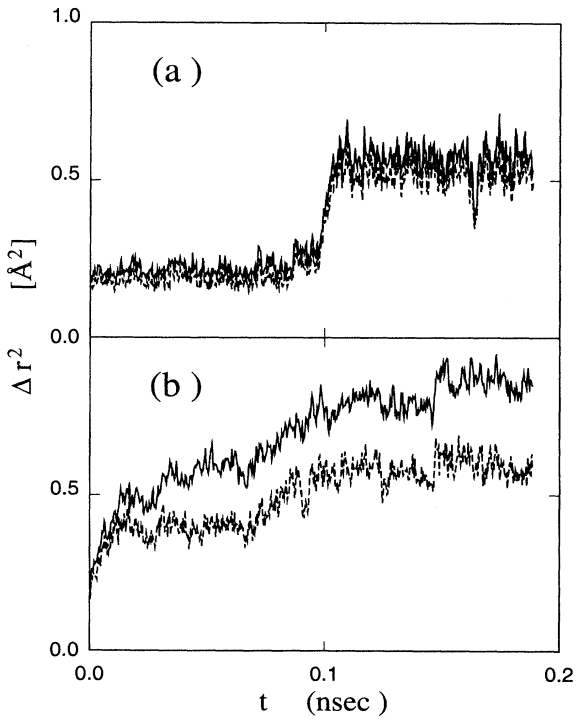

FIG. 4. Mean atomic displacement Δr^2 as a function of time for (a) crystalline $Ni_{80}Si_{20}$ at $T = 1341$ K, (b) amorphous $Au_{80}Si_{80}$ at $T = 398$ K. Solid line: metal atoms. Dashed line: Si atoms.

Despite the much lower T, it is possible to observe an almost continuous sequence of small jumps (again cooperative, as pointed out by the analysis of the atomic positions), producing a time evolution of Δr^2 that is much more gradual, and that reminds us of plastic flow.

Several recent experimental papers (see for instance Refs. 35 and 39) have discussed the validity for metallic glasses of the Einstein-Stokes relation

$$\eta D = \frac{k_b T}{6\ \pi r}, \tag{13}$$

where r is a length of the order of the atomic size. The apparent conclusion is that ηD is few orders of magnitude larger than what can be expected by extrapolating the high-T values, or, equivalently, r is much shorter than a typical atomic or ionic radius. Although the large error bars in our data at low T prevent a quantitative and reliable analysis, we point out that we observe a similar behavior in our simulation. By using Eq. (13) to compute r from η and D for $Pt_{80}Si_{20}$, we find that, starting from $\sim$ 0.8 Å at high T, r grows slowly to $\sim$ 1.2 Å where it drops discontinuously by one order of magnitude (see Fig. 5).

STATIC STRUCTURE

The partial radial distribution functions $g_{ij}(r)$ and the structure factors $S_{ij}(k)$ of the glassy alloys at room temperature have been computed as averages over 0.16 nsec MD runs. The results for $Pd_{80}Si_{20}$ are reported in Figs. 6 and 7, together with the available experimental data.[40]

The model has not been fitted to reproduce the details of the static structure of each compound, but to give an

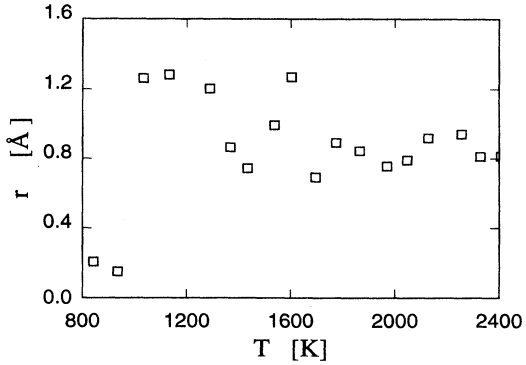

FIG. 5. Effective interatomic radius r for $Pd_{80}Si_{20}$ computed from the Einstein-Stokes relation, Eq. (13).

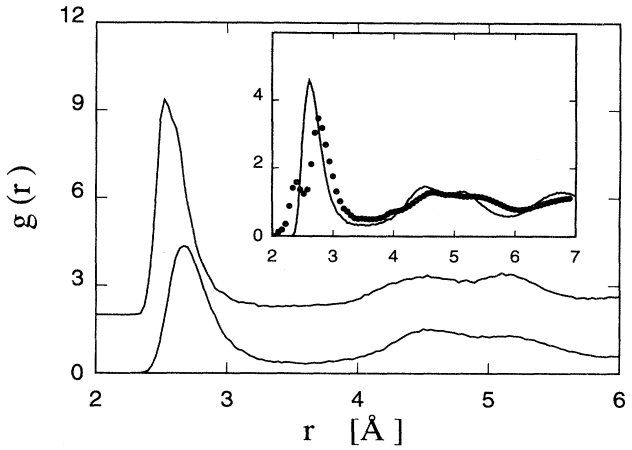

FIG. 6. Partial radial distribution functions for $Pd_{80}Si_{20}$ at 311 K. Lower curve: $g_{Pd\text{-}Pd}(r)$. Upper curve (shifted by two units): $g_{Pd\text{-}Si}(r)$. Inset: total radial distribution function. Solid line: present computation. Dots: neutron diffraction results.

overall reliable description of these systems. As a consequence, some disagreement is apparent in the $g(r)$ and $S(k)$, which, however, still reproduce the main features observed experimentally. The most important quantitative disagreement concerns the metal-metal and metal-metalloid nearest neighbor distance. In both the Pd-Si and Au-Si alloys (the only alloys for which experimental data are available) our EA potential overestimates the metal-Si NN distance by 3.5%, while the metal-metal NN distance is underestimated by almost the same fraction ($\sim$ 3.2%). As a result, the first peak in the total $g(r)$ is broad and cannot be resolved in the M-Si and M-M contributions, while the first peak of the experimental $g(r)$ presents a characteristic pre-peak due to the M-Si correlation. The errors in the M-Si and M-MNN distances are probably related, since the formation of a close bond between the M and Si would weaken the direct M-M bond. However, a significantly shorter M-Si bond is hard to achieve within the basic EA scheme we employed [unless we modify the simple prescription for the cross interaction, Eq. (2)], and we think that the error in the NN distances points to a deviation of the bonding from a purely metallic one. In fact, despite the overall metallic character of the system, it is not difficult to imagine that a small covalent component (directional, and involving the hybridization of the p levels of Si with the d of the metal) is also present,[41,20] and responsible for the short M-Si distance.

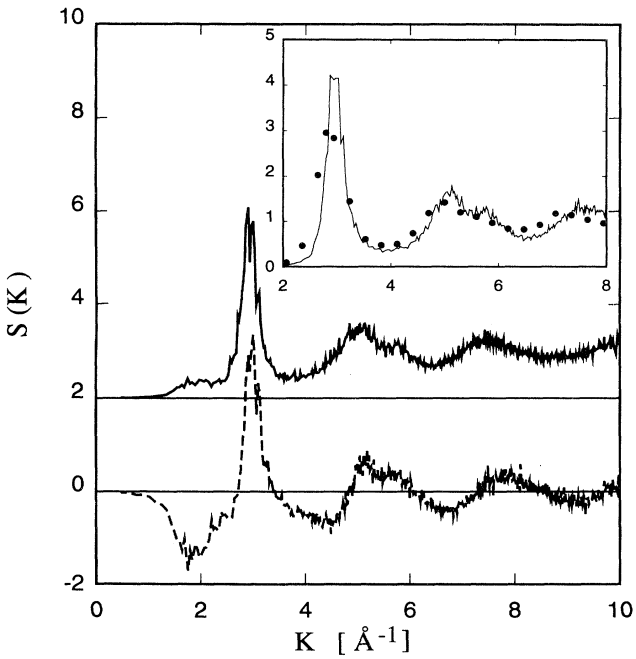

FIG. 7. Partial structure factors for $Pd_{80}Si_{20}$ at 311 K. Lower curve: $S_{Pd\text{-}Si}(K)$. Upper curve (shifted by two units): $S_{Pd\text{-}Pd}(K)$. Inset: total structure factor. Solid line: present computation. Dots: neutron diffraction results.

The error in the NN distances described above is reflected in the structure factor. Since the experimental partial $S_{ij}(K)$ are too noisy, we limit our comparison to the total $S(K)$. It is apparent that the computed $S(K)$ oscillates with a period that is $\sim$ 3% larger than the experimental one, corresponding to the EA underestimation of the M-M NN distance [$S(K)$ reflects mainly the behavior of $S_{M\text{-}M}(K)$]. Moreover, since the M and Si are more symmetric than in reality, the simulated system is markedly more ordered than its experimental counterpart, as shown by the higher first peak in $S(K)$ and by the slower decay of the successive oscillations.

To assess the importance of these discrepancies in the NN distances, we point out that for transition metals errors of the order of $\sim$ 2% are not uncommon in density functional theory in the local density approximation[42] (the state of the art in total energy-structural computations) and the 3.5% error of the EA potential is the price to be paid to allow extensive and inexpensive MD simulations. We also underline that the global description of the experimental structure provided by the EA potential is comparable and often better than that of other models (like second-order perturbation theory and TB models), including those requiring more extensive fitting.

In fact, despite the (important) quantitative discrepancies described above, the EA potential reproduces remarkably well all the features associated to the amorphous structure, as can be appreciated also by contrasting with the results for $Ni_{80}Si_{20}$, i.e., the system that crystallized during the quench (see Fig. 8). In agreement with the experimental results, our amorphous alloys display a strong chemical short-range order, as revealed by the negligible number of NN Si-Si pairs (a few units at most in each system). For all the amorphous and liquid systems the number of M atoms surrounding each Si is 9.9 ± 0.8 (Ref. 43) and remains almost constant over a wide temperature range. The average number of M atoms surrounding each other M atom is slightly more variable, ranging (at room temperature) from 9.8 ± 1 in $Au_{80}Si_{20}$ to 10.5 ± 1 in $Pt_{80}Si_{20}$, and decreasing with increasing temperature. The total coordination number (M plus Si) of the metal atoms in the amorphous alloys

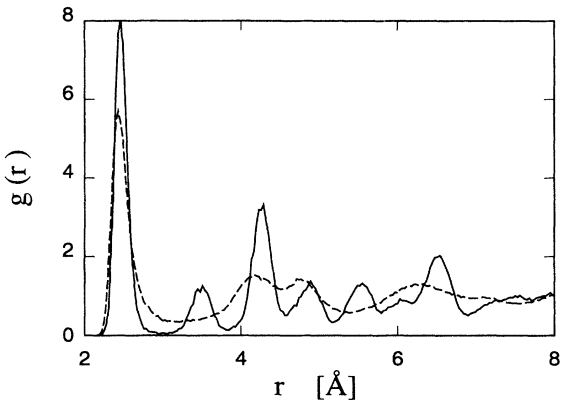

FIG. 8. Radial distribution function for $Ni_{80}Si_{20}$ at 300 K. Solid line: defective crystal structure obtained by the quench at 0.8 10^{12} K/sec. Dashed line: amorphous structure obtained by the quench at 10^{15} K/sec.

is close to 13, to be compared with the 12 computed for the crystallized $Ni_{80}Si_{20}$. A direct comparison of coordination numbers with experiments is difficult, since even for the most studied system ($Pd_{80}Si_{20}$) quantitative data are scarce and contradictory. For instance, the number of M neighbors of the Si atoms quoted in Ref. 44 (neutron diffraction data) is 6.6, while in Ref. 45 (neutron and x-ray diffraction) it is 9 ± 0.9. This second value is considered the most reliable, and is consistent with our results.

The first coordination shell of Si is better defined than that of the M atoms, as shown by the first peak of the partial $g_{ij}(r)$, which is higher and sharper for M-Si than for M-M. Both the $g_{M\text{-Si}}$ and $g_{M\text{-}M}$ present the characteristic asymmetry in the first peak (a slight shoulder beyond the maximum) that is usually associated with the strong chemical order of these systems and the trigonal prism geometry of the Si first coordination shell.[46] The second peak of $g(r)$ (partial and total) is split in a characteristic way, which becomes visible starting from ~ 200 K beyond T_g. The transition occurs when the ratio of the first peak to the first minimum reaches 14, which is the value predicted by the Wendt-Abraham[47] criterion.

Related features can be observed in the structure factor. The chemical order is apparent by constructing the concentration-concentration structure factor[48]

$$S_{CC}(K) = x_M x_{Si}[S_{M\text{-}M}(K) + S_{Si\text{-}Si}(K) - 2S_{Si\text{-}M}(K)], \tag{14}$$

where x_M and x_{Si} are the metal and Si concentrations, respectively. $S_{CC}(K)$ has a well-defined pre-peak (i.e., before the first peak), corresponding to the length scale of the first coordination shell. The second peak of $S(K)$ is asymmetric, with a pronounced shoulder on its high-K side.[40]

To investigate the dependence of the amorphous structure on the cooling rate we quenched abruptly a sample of each alloy from ~ 2000 K to room temperature. Since stabilizing the system at the final T requires ~ 1000 MD steps (or 1.6 psec), this process provides a cooling rate of 10^{15} K/sec, i.e., 1000 times faster than the slowest quench we described before. The systems that are amorphous after both quenches (i.e., all but $Ni_{80}Si_{20}$) present structures that are qualitatively similar in the two cases, with, however, quantitative differences that are easy to predict. The density achieved by the slow quench is 1.4% higher than for the fast one; that is, more defects are annealed in the slow process, whose total volume corresponds to roughly 12 atoms for our 864 atoms system. The $g(r)$ is similar in the two cases, with quantitative differences that are more apparent near the first minimum and the second peak: The first minimum is better defined, and the second peak is more clearly split and asymmetric in the slowly quenched systems. Room temperature diffusion is also significantly higher in the rapidly quenched systems, while it is barely detectable in the others.

The Voronoi construction has often been used to characterize the local symmetry in amorphous systems.[3] We carried out this analysis using standard library routines[31] for the amorphous alloys at zero and room temperature, and for liquid configurations close to T_g and at high temperature (~ 1500 K). A common characterization of the Voronoi polyhedra distribution is in terms of the numbers n_3, n_4, n_5, ... of polyhedra faces having $3, 4, 5, \ldots$ edges.[49] As remarked by several previous studies, this characterization produces a very large number of different (n_3, n_4, n_5, ...) signatures, and fails to provide a clear and synthetic picture of the local arrangement. Easier to interpret is the probability distribution of faces with n edges. In our three zero-temperature amorphous systems pentagonal faces dominate, representing roughly 50% of the total faces, and highlighting the importance of local fivefold symmetry. Ideal icosahedral arrangements (i.e., Voronoi polyhedra with 12 pentagonal faces), however, are extremely rare. With increasing temperature the relative importance of pentagonal faces decreases in favor of the hexagonal ones. The same trend is observed in zero-temperature samples obtained by a fast quench from high T. These trends suggest that the local fivefold symmetry is a peculiar structure dominating the low-temperature undercooled liquid more than a remnant of the equilibrium liquid phase. The NN shell for the Si atoms that are ninefold coordinated is usually recognizable as the triangular prism unit (Fe_3C cementite) that has been often invoked to explain the Si coordination in these systems, and the shape of the first peak of $g(r)$.

To characterize the medium-range order on the scale of 10–15 Å we studied the properties of approximate square paths going through NN atoms. The paths were started from a given atom i by selecting at random the direction $\hat{n}$ connecting i to one of its neighbors in the first coordination shell. One side of the square was then constructed by repeating m times ($m = 3, 4, 5$), this basic step joining NN atoms in such a way as to conserve as much as possible the original direction $\hat{n}$. A sequence of four sides separated by (approximate) clockwise 90° turns defines our approximate square path. In a perfect cubic crystal this procedure returns to the starting atom. In defective crystals this algorithm provides a way to identify dislocations. The distance $\vec{b}$ between the final and the starting point is the defect's Burger vector.

Our systems are too small and too disordered to allow a clear definition of dislocations. Despite this limitation we use the dislocation terminology to discuss the properties of the square paths described above. As a benchmark for the glassy systems we first discuss the results for the defective $Ni_{80}Si_{20}$ crystal obtained by our annealing and one undercooled liquid system ($Pd_{80}Si_{20}$ at $T = 1066$ K) (see Fig. 9). In $Ni_{80}Si_{20}$ at room temperature the majority of the paths returns to the starting point ($\vec{b} = 0$). Most of the remaining paths end up in one of the NN's of the starting atom. Only very few end up in the second and third NN. When nonzero, the orientation of $\vec{b}$ is isotropic. In the undercooled $Pd_{80}Si_{20}$ at $T = 1066$ K most of the paths do not close. The probability distribution $P(|\vec{b}|)$ for the length of $\vec{b}$ has one broad peak at the NN distance, but all the other distances are represented up to at least the third NN. The orientation of $\vec{b}$ displays a small but statistically significant preference for orientations perpendicular to the plane of the path. In the language of dislocations, screw dislocations are more common than edge dislocations. The situation in the glassy samples is intermediate between these two cases: The peak in $P(|\vec{b}|)$ at the NN distance is higher and sharper than in the liquid, but $P(|\vec{b}|)$ decays slowly with distance. The preferential polarization of $\vec{b}$ perpendicular to the plane of the path is even stronger than in the liquid, although the difference between the two is at the limit of the statistical error.

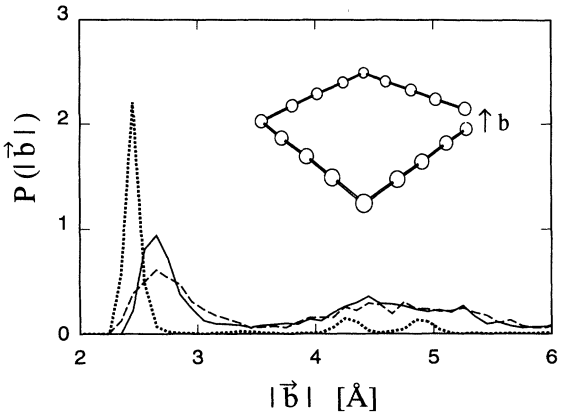

FIG. 9. Probability distribution for the modulus of the Burger's vector **b** for square loops spanning four nearest neighbor atoms. Solid line: glassy $Pd_{80}Si_{20}$ at T308 K. Dashed line: liquid $Pd_{80}Si_{20}$ at $T = 1066$ K. Dotted line: defective $Ni_{80}Si_{20}$ crystal at $T = 295$ K. The area under the curves is normalized to one. A peak at $|\vec{b}| = 0$ is not displayed in the figure.

ELASTIC PROPERTIES

Before computing the elastic constants, we verified that the cubic shape of the cell imposed during the quench is stable by relaxing the system at zero pressure within the Parrinello-Rahman method, which allows the simulation cell to change shape as well as volume. A long relaxation at room temperature did not produce any significant variation in the simulation cell. This allows us to compute the elastic constants with the constraints and simplifications appropriate for cubic systems. The bulk modulus B and the elastic constants C_{11}, C_{12}, and C_{44} have been determined by the energy variation under the deformations of the unit cell described in Ref. 50. After applying each deformation (with up to 1% variation in each of the sides) the position of the atoms within the cell has been accurately relaxed. The results, reported in Table VI, are in good agreement with the few available experimental data.[51] As expected for amorphous systems, the computed elastic constants satisfy the relation $C_{11} = C_{12} + 2C_{44}$ which is implied by the system isotropy. The significance of this relation is highlighted by the result for $Ni_{80}Si_{20}$, which violates it by more than 20%.

The phonon density of states (DOS) of the amorphous alloys has been computed by direct diagonalization of the dynamical matrix for the 864-atom systems, after a careful relaxation of the atomic positions. Because of the relatively large system size, we considered only the Γ point of the Brillouin zone associated with the periodically repeated simulation cell. The computation provided both the vibrational frequencies $\nu^{(\alpha)}$ and the normalized eigenvectors $\vec{B}_i^{(\alpha)}$, where α labels the modes and i the atoms. The DOS for $Au_{80}Si_{20}$, which is representative of those for the other systems, is reported in Fig. 10 together with the corresponding DOS for pure fcc gold. The comparison of these two curves shows that our model reproduces the two major features of the DOS for the amorphous metal-metalloid glasses observed in experiments:[52] (i) A wide band extending beyond the high-frequency edge of the pure metal; (ii) an enhancement of the low-frequency part of the alloy DOS with respect to that of the pure metal. The analysis of phonon localization via the participation ratio[53]

$$p^{(\alpha)}(\nu_\alpha) = \frac{N\left[\sum_{i=1}^{N} |\vec{B}_i^{\alpha}(\nu_\alpha)|^2\right]^2}{\sum_{i=1}^{N} |\vec{B}_i^{\alpha}(\nu_\alpha)|^4} \qquad (15)$$

TABLE VI. Bulk modulus B, elastic constants C_{ij}, and Poisson's ratio ν for the amorphous alloys $Pd_{80}Si_{20}$, $Pt_{80}Si_{20}$, $Au_{80}Si_{20}$, and the defective fcc crystal $Ni_{80}Si_{20}$ at room temperature.

	B (Mbar)	C_{11} (Mbar)	C_{12} (Mbar)	C_{44} (Mbar)	ν
$Ni_{80}Si_{20}$	1.77	3.44	0.94	1.62	0.44
$Pd_{80}Si_{20}$	1.90	2.43	1.63	0.22	0.40
$Pt_{80}Si_{20}$	2.69	3.26	2.40	0.42	0.42
$Au_{80}Si_{20}$	1.70	2.00	1.55	0.22	0.44

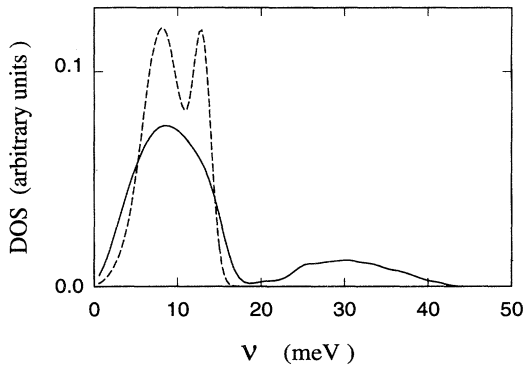

FIG. 10. Vibrational density of states. Solid line: amorphous $Au_{80}Si_{20}$, $T = 318$ K. Dashed line: fcc Au, $T = 0$ K.

shows that, as easily predicted, the high-frequency band is due to very localized modes, involving almost exclusively Si atoms (see Fig. 11). The excess low-frequency modes induced by Si alloying in the range 2 meV $\leq \nu \leq 5$ meV are associated mainly with the displacement of the metal atoms, with only a relatively small component on Si. Finally, the few (~5–10) relatively localized modes at $\nu = 1.5$ meV are worthy of mention. They are apparently related to the quasilocalized (or resonant) modes described by Laird and Schober in the case of a simple model glass:[54] In common with the excitations described by these authors, they occupy the low-frequency tail of the DOS, involve the motion of ~ 20–30 atoms (as displayed by their participation ratio of 0.1–0.2), and they are highly anharmonic, as shown by their large Grüneisen parameter (see the inset of Fig. 11). All these features suggest an identification of these modes with the characteristic and universal low-temperature excitation of glasses, and, in particular, suggest a connection with the "soft potential model" introduced in Ref. 55 to provide a unified description of tunneling modes (relevant at $T \sim 1$ K), harmonic quasilocalized modes (T ~2–5 K), and thermally activated relaxation ($T \sim 20$ K). A note of caution, however, is in order, since the small size of our

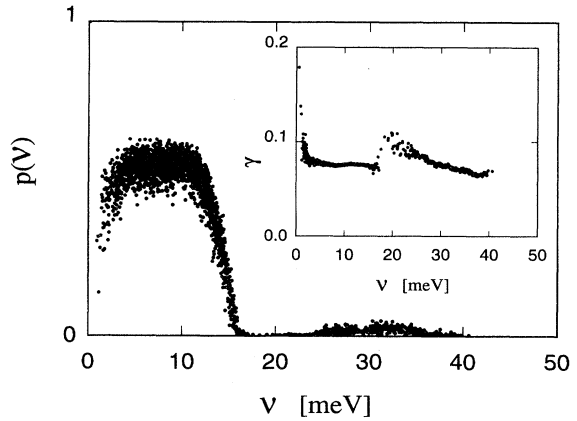

FIG. 11. Phonon participation ratio (see text) for $Au_{80}Si_{20}$, $T = 318$ K. Inset: Grüneisen parameter for the same system.

systems makes very unlikely the inclusion in our samples of the tunneling modes with energies around 1 K, and also in the energy range up to 20 K our sampling of the DOS is limited to few modes.

An alternative description of the local elastic properties of an amorphous system can be obtained via the computation of the atomic stress, along the lines proposed in Ref. 56. The atomic stress $\sigma^i_{\alpha\beta}$ at atom i is defined by Eq. (8) above. The sum of $\sigma^i_{\alpha\beta}$ over the atoms provides the virial tensor of the system. The trace $\sigma^i = (\sigma^i_{xx} + \sigma^i_{yy} + \sigma^i_{zz})/3$ defines a local pressure on the atom i, while the mean square deviation τ_i (von Mises shear stress),

$$\tau_i = \left[\frac{1}{3}\left(\frac{(\sigma^i_{xx} - \sigma^i_{yy})^2}{2} + \frac{(\sigma^i_{xx} - \sigma^i_{zz})^2}{2} + \frac{(\sigma^i_{yy} - \sigma^i_{zz})^2}{2}\right)\right]^{1/2}, \tag{16}$$

measures the anisotropy of the local stress. Both quantities are identically zero for a monoatomic Bravais lattice at zero pressure. We computed σ_i and τ_i for liquid and amorphous systems, averaging over few independent configurations. The results are summarized by the probability $P(\sigma)$ [or $P(\tau)$] for an atom to experience the local stress σ (or von Mises shear stress τ). The distribution $P(\sigma)$ for $Au_{80}Si_{20}$ is displayed in Fig. 12. In the liquid

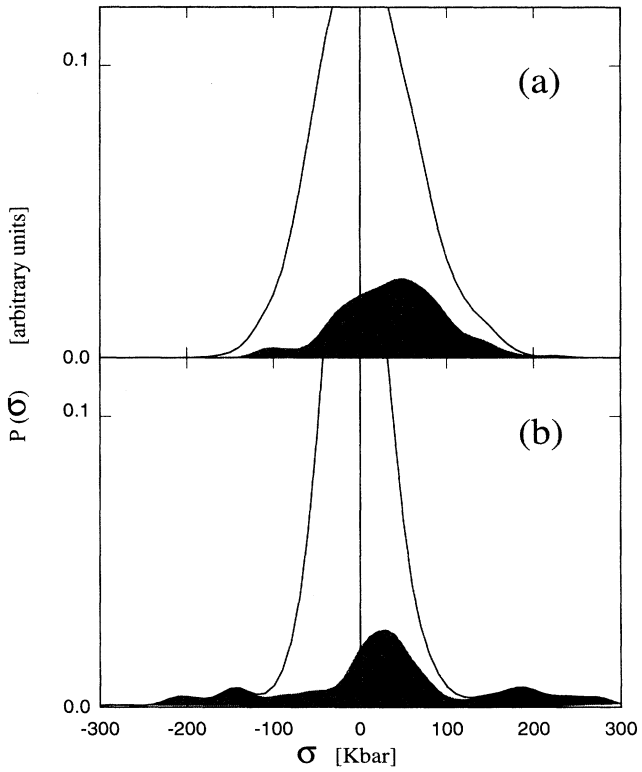

FIG. 12. Probability distribution P for the hydrostatic atomic stress σ in (a) undercooled liquid $Au_{80}Si_{20}$, $T = 818$ K; (b) amorphous $Au_{80}Si_{20}$, $T = 318$ K. The shaded area represents the probability distribution restricted to the Si atoms.

state the distribution is rather broad, covering $\sim$ 400 kbar, almost symmetric with respect to the origin, and the distributions for the Si and Au atoms are similar. The situation changes rapidly with T decreasing below T_g: While the distribution for Au becomes significantly narrower (with possibly a slight asymmetry toward negative σ), the distribution for Si develops long tails, extending (slightly asymmetrically) up to 300 kbar. Similar results are obtained for $P(\tau)$, showing that the stress accumulating at the Si atoms becomes highly anisotropic. This behavior is reminiscent of the picture for the glass transition proposed by Egami and Vitek in Ref. 57, identifying the transition with the percolation through the system of orientationally coordinated stresses. The feature peculiar to our system is that high stresses reside on Si only, while the temperature dependence of $P(\sigma)$ for the metal follows the normal trend toward a narrow distribution centered around the origin.

CONCLUSIONS

Alloys of late transition metals with up to 20 at.% of Si are experimentally known to be metallic. On the basis of this observation, we propose to apply the well-known embedded-atom method to provide a simple and computationally convenient description of glass-forming metal-Si alloys. We produced a potential able to describe alloys of Al, Ni, Pd, Pt, and Au with Si. The potential for the metals has been constructed following standard procedures, described in Refs. 16 and 26. The potential for Si has been based on *ab initio* results for the lattice parameter, the cohesive energy, the bulk modulus, and the elastic constants of the metastable simple cubic phase.[27] The cross interaction between Si and the metals has been constructed by first gauging the interaction potentials of the metals among themselves and then by adjusting carefully the interaction of Si with one of the metals. As the reference metal for this last step we choose Al because of the expected similarity in size and chemical behavior of Al and Si in a metallic environment. The reliability of our procedure in describing alloys whose properties have not been fitted has been tested by performing computations for several metal-rich ordered silicides. The results show that our model, although not quantitatively accurate, is remarkably robust in providing the qualitative features and the trends in a large class of alloys.

The model has been exploited to simulate by MD the quench from high T of 864-atom samples of $Ni_{80}Si_{20}$, $Pd_{80}Si_{20}$, $Pt_{80}Si_{20}$, and $Au_{80}Si_{20}$. A cooling rate of 0.8×10^{12} K/sec gives rise to amorphous structures for the Pd-, Pt-, and Au-Si alloys, while Ni-Si crystallizes. This is in agreement with the observation that this last system is not produced in the amorphous state by a thermal process unless a third element (like Ge or P) is added. The glass transition temperature T_g, determined by the discontinuity in the slope of $U(T)$, reproduces the experimental trends, despite an overestimation of $\sim$ 200 K, which is at least partially due to the fast quenching rate imposed by MD.

The static structure of the amorphous alloys, characterized by the partial radial distribution functions and structure factors, displays the major features observed in the experimental results. The first peak of the M-M and M-Si $g(r)$ is asymmetric, with a characteristic shoulder after the maximum. The second peak is split, and this feature appears $\sim$ 200 K beyond T_g. The glass transition occurs when the ratio of the maximum to the first minimum in the total $g(r)$ approaches 14, in agreement with the empirical Wendt-Abraham law. The Si-Si nearest neighbor pairs are rare (metalloid-metalloid avoidance), and the analysis of the first coordination shell of Si highlights the importance of the triangular prism unit often associated to the ninefold coordination of the metalloid and the asymmetry in the first peak of $g(r)$. As already observed in the case of the ordered alloys, the model is not quantitatively accurate in describing the details of the structure: The M-Si NN distance is underestimated, and the M-M NN distance is overestimated, both by $\sim$ 3%.

The model has also been used to study a variety of transport and dynamical properties of the alloys in the liquid and amorphous phases. The diffusion coefficient D and the viscosity η display a clear Arrhenius behavior in the liquid phase. Approaching T_g our estimate for these two quantities becomes less reliable, but shows that they change rather smoothly across the glass transition. The product $D\eta$, which, according to Stoke's law is inversely proportional to a characteristic atomic size, has a more discontinuous change at T_g, where it decreases by roughly one order of magnitude.

The analysis of the vibrational properties shows that the model reproduces the major features of the experimental DOS for the amorphous metal-metalloid glasses: The Si alloying and the subsequent amorphization induce an excess of low-frequency phonons associated with the displacement of the metal atoms, and a wide band of high-frequency localized modes involving the movement of the Si atoms only. Few quasilocalized modes at the low-frequency tail of the DOS provide the connection between our simulation and recent theoretical discussions of the characteristic and universal vibrational properties of glasses.

An intriguing microscopic view of the glass transition is provided by the computation of the atomic stresses, showing that with decreasing temperature, and starting from T_g a large and highly anisotropic stress is trapped at the Si atoms.

All these results show that the model reliably describes a variety of structural and dynamical properties of M-Si glass-forming alloys. Moreover, due to the intrinsic reliability of the EA potential in describing inhomogeneous systems, the model is particularly suitable for the investigation of surfaces and interfaces of metallic alloys. It can also be easily extended to ternary and multicomponent systems, which are indeed the ones with the most promising technological applications and that, moreover, include intriguing examples of quasicrystals.

ACKNOWLEDGMENTS

We thank Stefano de Gironcoli for the *ab initio* computation of structural and elastic properties of simple cubic

silicon. We acknowledge H. R. Schober for useful discussions and a careful reading of the manuscript.

APPENDIX

To reproduce faithfully the properties of Si in a metallic environment we fit our EA potential on the properties of one of the various metallic phases of Si, which become stable under high pressure.[58,59] Since the structural and elastic properties required to determine such a potential are not available from experiments, we rely on *ab initio* computations within a density-functional-theory local density approximation (DFT LDA).[27] We base our computation on the simple cubic phase because of its simplicity and because its (metastable) equilibrium volume per atom is the closest to the equilibrium volume of fcc Al. The computation of the equilibrium volume V_0, cohesive energy E_0, and the elastic properties has been performed by using pseudopotentials[60] and a plane wave expansion for the Kohn-Sham orbitals. The Brillouin zone has been sampled with 56 special **k** points in its irreducible wedge,[61] and the broadening technique[62] has been used to deal with the metallic nature of the system. For the broadening function a first-order Hermite-Gaussian function[63] has been chosen, which makes quite insensitive the result on the value of the Gaussian width used. The elastic constants have been evaluated by taking the numerical derivative of the stress tensor[64] for two independent uniaxial deformations of the crystal [along the (001) direction for C_{11} and C_{12} and along the $(1\bar{1}1)$ direction for C_{44}]. In view of the well-known overestimation of E_0 by the DFT LDA, the difference between the cohesive energy of the simple cubic and diamond phases has been computed, and added to the experimental E_0 for diamond Si.

The potential parameters for Si have then been determined by the usual procedure, with two exceptions. First, the Murnaghan equation of state[65]

$$E(V) = E_0 + \frac{B_0 V}{B_0'(B_0'-1)}[B_0'(1-V_0/V) + (V_0/V)^{B_0'} - 1] \quad \text{(A1)}$$

(with $E_0 = 4.30$ eV/atom, $V_0 = 15.96$ Å^3, the bulk modulus $B_0 = 1.04$ Mbar, and its pressure derivative $B_0' = 4$) reproduces the *ab initio* equation of state better than the one by Rose *et al.*[66] (that was used for Al and the TM's), and has been applied to compute the embedding function $F[\rho]$ for Si in a range of densities around the equilibrium one. Second, we did not fit the vacancy formation energy, because this quantity has not been determined in the *ab initio* computation.

The parameter n_α for Si has been determined by fitting the lattice constant of Al:Si fcc random alloys. The results of this fit and a short discussion are reported in Ref. 25. To prevent any possible instability, a short-range repulsive potential has been added to Si at distances shorter than those included in the fit ($r < 2.4$ Å).

As stressed above, this simple potential was not intended to reproduce the variety of phases Si displays, encompassing both covalent and metallic bonding. However, to determine the range of validity of our model, it is useful investigate how it describes the Si phases other than the simple cubic. The β-tin structure is metallic, with a volume per atom very close to that of the sc phase. Not surprisingly, our model reproduces well both its cohesive energy ($E_0 = 4.20$ eV/atom computed by the EA potential, vs the *ab initio* value $E_0 = 4.35$) and the lattice parameter ($a = 4.848$ Å, $c = 2.454$ Å in the EA potential, vs the *ab initio* $a = 4.82$ Å, $c = 2.66$ Å), with only a slight distortion in the atomic positions. More demanding is the diamond structure, which is semiconducting. We find that our model has diamond as a metastable structure, with a cohesive energy $E_0 = 4.65$ eV/atom (experimental $E_0 = 4.63$ eV/atom), a lattice parameter $a = 5.64$ Å that is 4% larger than the experimental one ($a = 5.43$ Å), and elastic constants close to those obtained in Ref. 23. The metastability range of this structure is rather extended, since it does not transform during a long MD run (160 psec) at $T \sim 500$ K. Only beyond this temperature does it spontaneously transform to a different, distorted structure that we have been unable to identify. This last structure, which we assume is the model ground state, has a cohesive energy $E_0 = 4.75$ eV/atom and is fourfold coordinated.

We stress that, despite the qualitative similarity of the phases displayed by our model and the experimental or *ab initio* Si, we do not expect our potential to be reliable for Si outside the narrow range of metallic alloys that are the subject of our study. In particular, we did not check properties like defect or surface energies for pure Si, and we have no reason to expect the model to be accurate.

[1] See, for instance, *Glassy Metals III*, edited by H. Beck and H.-J. Güntherodt (Springer-Verlag, Heidelberg, 1994).
[2] W. Götze and L. Sjögren, Rep. Prog. Phys. **55**, 241 (1992); A. Hunt, J. Non-Cryst. Solids **160**, 183 (1993).
[3] F. Yonezawa, in *Solid State Physics*, edited by H. Ehrenreich and D. Turnbull (Academic Press, San Diego, 1991), Vol. 45, p. 179.
[4] R. W. Cahn, in *Glasses and Amorphous Materials*, Material Science and Technology Vol. 9, edited by J. Zarzycki (VCH, Weinheim, 1991), p. 493.
[5] L. V. Woodcock and C. A. Angell, Phys. Rev. Lett. **47**, 1129 (1981).
[6] A. Rahman, M. J. Mandell, and J. P. McTague, J. Chem. Phys. **64**, 1564 (1976).
[7] B. Bernu, J. P. Hansen, Y. Hiwatari, and G. Pastore, Phys. Rev. A **36**, 4891 (1987).
[8] R. G. Della Valle *et al.*, Phys. Rev. B **49**, 12 625 (1994).
[9] J. Hafner, *From Hamiltonians to Phase Diagrams*, Vol. 70 of *Springer Series in Solid State Sciences* (Springer, Berlin, 1987).
[10] L. von Heimendahl, J. Phys. F **9**, 161 (1979).
[11] R. N. Barnett, C. L. Cleveland, and U. Landmann,

Phys. Rev. Lett. **55**, 2035 (1985); S. S. Jaswal and J. Hafner, Phys. Rev. B **38**, 7311 (1988).
[12] S. S. Jaswal and J. Hafner, Phys. Rev. B **38**, 7320 (1988).
[13] Ch. Hausleitner and J. Hafner, Phys. Rev. B **45**, 115 (1992); **45**, 128 (1992).
[14] Ch. Hausleitner, M. Tegze, and J. Hafner, J. Phys. Condens. Matter **4**, 9557 (1992).
[15] Ch. Hausleitner and J. Hafner, Phys. Rev. B. **47**, 5689 (1993); Ch. Hausleitner, J. Hafner, and Ch. Becker, *ibid.* **47**, 13 119 (1993).
[16] M. S. Daw and M. I. Baskes, Phys. Rev. Lett. **50**, 1285 (1983); Phys. Rev. **29**, 6443 (1984).
[17] We include in the same EA category the equivalent effective medium potentials [K. W. Jacobsen, J. K. Nørskov, and M. J. Puska, Phys. Rev. B **35**, 7423 (1987)] and the second moment approximation to TB models [V. Rosato, M. Guillope, and B. Legrand, Philos. Mag. A **59**, 321 (1989)].
[18] C. Massobrio, V. Pontikis, and G. Martin, Phys. Rev. B **41**, 10 486 (1991).
[19] C. S. Becquart, P. C. Clapp, M. V. Glazov, and J. A. Rifkin, Comput. Mater. Sci. **1**, 411 (1993).
[20] J. D. Riley *et al.*, Phys. Rev. B **20**, 776 (1979); K. Tanaka *et al.*, *ibid.* **32**, 6853 (1985).
[21] E. Huber and M. von Allmen, Phys. Rev. B **28**, 2979 (1983); **31**, 3338 (1985).
[22] J. Chevrier, D. Pavuna, and F. Cyrot-Lackmann, Phys. Rev. B **36**, 9115 (1987).
[23] M. I. Baskes, Phys. Rev. Lett. **59**, 2666 (1987).
[24] A. E. Carlsson, P. A. Fedder, and C. W. Myles, Phys. Rev. B **41**, 1247 (1990).
[25] S. Rubini and P. Ballone, Phys. Rev. B **50**, 9648 (1994).
[26] S. M. Foiles, M. I. Baskes, and M. S. Daw, Phys. Rev. B **33**, 7983 (1986).
[27] S. de Gironcoli (private communication).
[28] M. Hansen, *Constitution of Binary Alloys*, 2nd ed. (McGraw-Hill, New York, 1958).
[29] R. Hultgren, P. D. Desai, D. T. Hawkins, M. Gleiser, and K. K. Kelley, *Selected Values of Thermodynamical Properties of Binary Alloys* (American Society for Metals, New York, 1973).
[30] J. Zou and A. E. Carlsson, Phys. Rev. B **50**, 99 (1994); **47**, 2961 (1993).
[31] M. P. Allen and D. J. Tildesley, *Computer Simulation of Liquids* (Clarendon Press, Oxford, 1989).
[32] von Allmen, in *Glassy Metals II*, edited by H. Beck and H.-J. Güntherodt (Springer-Verlag, Heidelberg, 1983); some estimates of the cooling rate in laser quenching are as high as 10^{12} K/sec: C.-J. Lin and F. Spaepen, in *Rapidly Solidified Metastable Materials*, edited by B. H. Keav and B. C. Giessen, MRS Symposia Proceedings No. 28 (Material Research Society, Pittsburgh, 1984), p. 75.
[33] M. Parrinello and A. Rahman, J. Appl. Phys. **52**, 7182 (1981).
[34] L. Battezzati and A. L. Greer, Acta Metall. **37**, 1791 (1989).
[35] A. L. Greer, J. Non-Cryst. Solids **61-62**, 737 (1984).
[36] U. Bengtzelius, W. Götze, and A. Sjölander, J. Phys. C **17**, 5915 (1984).
[37] H. R. Schober and B. B. Laird, Phys. Rev. B **44**, 6746 (1991).
[38] D. Turnbull and M. H. Cohen, J. Chem. Phys. **29**, 1049 (1958); **34**, 120 (1961). See also Ref. 3 for a discussion of the validity of the free volume theory in amorphous systems.
[39] A. W. Wagner and F. Spaepen, Mater. Sci. Eng. A **179-180**, 265 (1994).
[40] T. Fukunaga and K. Suzuki, Sci. Rep. Res. Inst. Tohoku Univ. A **29**, 153 (1981); **28**, 208 (1980).
[41] J. F. van Acker, E. W. Lindeyer, and J. C. Fuggle, J. Phys. Condens. Matter **3**, 9579 (1991).
[42] G. P. Srivastava and D. Weaire, Adv. Phys. **36**, 463 (1987).
[43] The *M-M*, *M*-Si, and Si-Si average coordination numbers are computed by integrating the partial $g(r)$'s up to their first minimum.
[44] T. Fukunaga, M. Misawa, T. Masumoto, and K. Suzuki, Sci. Rep. Res. Inst. Tohoku Univ. A **29**, 153 (1981).
[45] J. F. Sadoc and J. Dixmier, in *The Structure of Non-Crystalline Materials*, edited by P. H. Gaskell (Taylor & Francis, London, 1977).
[46] P. H. Gaskell, in *Amorphous Metals*, edited by H. Matyja and P. G. Zielinski (World Scientific Publishing, Singapore, 1986).
[47] H. R. Wendt and F. F. Abraham, Phys. Rev. Lett. **41**, 1244 (1978).
[48] A. B. Bathia and D. E. Thornton, Phys. Rev. B **2**, 3004 (1970).
[49] J. L. Finney, Proc. R. Soc. London A **319**, 479 (1970).
[50] J. E. Osburn, M. J. Mehl, and B. M. Klein, Phys. Rev. B **43**, 1805 (1991).
[51] H.-U. Künzi, in *Glassy Metals II* (Ref. 32).
[52] J.-B. Suck and H. Rudin, in *Glassy Metals II* (Ref. 32).
[53] R. J. Bell, P. Dean, and D. C. Hibbins-Butler, J. Phys. C **3**, 2111 (1970); W. M. Visscher, J. Non-Cryst. Solids **8-10**, 477 (1972).
[54] B. B. Laird and H. R. Schober, Phys. Rev. Lett. **66**, 636 (1991).
[55] V. G. Karpov, M. I. Klinger, and F. N. Ignat'ev, Sov. Phys. JETP **57**, 439 (1983); M. A. Il'in, V. G. Karpov, and D. A. Parshin, *ibid.* **65**, 165 (1987).
[56] T. Egami, K. Maeda, and V. Vitek, Philos. Mag. **41**, 883 (1980).
[57] T. Egami and V. Vitek, in *Phase Transitions in Condensed Systems—Experiments and Theory*, edited by G. S. Cargill III, F. Spaepen, and K. N. Tu, MRS Symposia Proceedings No. 57 (Materials Research Society, Pittsburgh, 1987), p. 199.
[58] M. T. Yin and M. L. Cohen, Phys. Rev. B **26**, 5668 (1982).
[59] R. Biswas, R. M. Martin, R. J. Needs, and O. H. Nielsen, Phys. Rev. B **35**, 9559 (1987).
[60] G. B. Bachelet, D.R. Hamann, and M. Schlüter, Phys. Rev. B **26**, 4199 (1982).
[61] H. J. Monkhorst and J. D. Pack, Phys. Rev. B **13**, 5188 (1976).
[62] C.-L. Fu and K.-M. Ho, Phys. Rev. B **28**, 5480 (1983).
[63] M. Methfessel and A. T. Paxton, Phys. Rev. B **40**, 3616 (1989).
[64] O. H. Nielsen and R. M. Martin, Phys. Rev. B **32**, 3792 (1985).
[65] F. D. Murnaghan, Proc. Natl. Acad. Sci. USA **30**, 5390 (1944).
[66] J. H. Rose, J. R. Smith, F. Guinea, and J. Ferrante, Phys. Rev. B **29**, 1963 (1984).